Northumbria Research Link

Citation: Rong, Huazhen, Guan, Yixing, Li, Jun, Li, Ziyi, Ma, Dan, Zhang, Jingjing, Liu, Xiaoteng and Zou, Xiaoqin (2022) Dual-templating surface gel into thin SSZ-13 zeolite membrane for fast selective hydrogen separation. Aggregate, 3 (6). e275. ISSN 2692-4560

Published by: Wiley-Blackwell

URL: https://doi.org/10.1002/agt2.275 <https://doi.org/10.1002/agt2.275>

This version was downloaded from Northumbria Research Link: https://nrl.northumbria.ac.uk/id/eprint/50263/

Northumbria University has developed Northumbria Research Link (NRL) to enable users to access the University's research output. Copyright © and moral rights for items on NRL are retained by the individual author(s) and/or other copyright owners. Single copies of full items can be reproduced, displayed or performed, and given to third parties in any format or medium for personal research or study, educational, or not-for-profit purposes without prior permission or charge, provided the authors, title and full bibliographic details are given, as well as a hyperlink and/or URL to the original metadata page. The content must not be changed in any way. Full items must not be sold commercially in any format or medium without formal permission of the copyright holder. The full policy is available online: http://nrl.northumbria.ac.uk/policies.html

This document may differ from the final, published version of the research and has been made available online in accordance with publisher policies. To read and/or cite from the published version of the research, please visit the publisher's website (a subscription may be required.)

Northumbria University NEWCASTLE

University Library

Received: 23 June 2022 | Revised: 1 September 2022 | Accepted: 6 September 2022

DOI: 10.1002/agt2.275

Aggregate Open Access WILEY

RESEARCH ARTICLE

Dual-templating surface gel into thin SSZ-13 zeolite membrane for fast selective hydrogen separation

Special Issue: Emerging Investigators

Huazhen Rong[1] | **Yixing Guan**[1] | **Jun Li**[2] | **Ziyi Li**[2] | **Dan Ma**[1] | **Jingjing Zhang**[1] | **Terence Xiaoteng Liu**[3] | **Xiaoqin Zou**[1]

[1]Faculty of Chemistry, Northeast Normal University, Changchun, China

[2]School of Energy and Environmental Engineering, University of Science and Technology Beijing, Beijing, China

[3]Department of Mechanical and Construction Engineering, Faculty of Engineering and Environment, Northumbria University, Newcastle Upon Tyne, UK

Correspondence
Xiaoqin Zou, Faculty of Chemistry, Northeast Normal University, Changchun 130024, China.
Email: zouxq100@nenu.edu.cn; xiaoqinzou123@gmail.com

Funding information
National Natural Science Foundation of China, Grant/Award Numbers: 21971035, 22131004, U21A20330; "111" Program, Grant/Award Number: B18012; Fundamental Research Funds for the Central Universities, Grant/Award Number: JGPY202103

Abstract

Highly permeable zeolite membranes are desirable for fast gas separation in the industry. Reducing the membrane's thickness is deemed to be an optimal solution for permeability improvement. Herein, we report the synthesis route of thin SSZ-13 zeolite membranes via the conversion of template-contained surface gels. The synthesis gel is fully crystallized into crack-free SSZ-13 membranes assisted with dual templates of *N*,*N*,*N*-trimethyl-1-adamantammonium hydroxide (TMAdaOH) and tetraethylammonium hydroxide (TEAOH). The specific functions of TMAdaOH for structure directing and TEAOH for crystallization regulating are well discussed. Thin surface gel layer is impregnated onto porous alumina with subsequent crystallization into a 500 nm thick membrane. This submicron-thick membrane exhibits high H_2 permeance with 50×10^{-8} mol s^{-1} m^{-2} Pa^{-1} during hydrogen separation. Meanwhile, the separation factors are retained around 23.0 and 31.5 for H_2/C_2H_6 and H_2/C_3H_8, respectively. This approach offers a possibility for obtaining high-quality zeolite membranes for efficient hydrogen separation.

KEYWORDS
gas separation, hydrogen selectivity, zeolite membrane

1 | INTRODUCTION

Membrane separation as a low energy-consumption technology has been widely used for gas separation, desalination, solvent recovery, and chemical production industries.[1–3] Membrane gas separation has attracted particular attention because it produces high-purity gases in a continuous mode.[4] Zeolite membranes are a special type of aggregates, in which zeolite crystals are closely and orderly assembled into continuous layers. Processing zeolites into membranes can fulfill their functions in gas separations. Zeolites are typical microporous inorganics and they have uniform pores in small sizes (3–10 Å).[5] The molecular-level pores are able to separate gas molecules from one another via molecular size, showing the capability of gas separation. In addition, zeolite membranes usually have excellent thermal/chemical stabilities and their surface properties are tunable.[6] Recently, eight-membered-ring zeolite membranes including CHA,[7–10] DDR,[11–14] LTA,[15,16] etc. have been explored for gas separations as the pore sizes of these zeolites below 4 Å which are particularly suitable for separating light gases, for instance, hydrogen separation.[17] Hydrogen is a clean and renewable resource with potential for alleviating the increasing environmental pollution and energy crisis. It is industrially produced via cracking or dehydrogenation of petroleum.[18,19] There are a range of hydrocarbon impurities as by-products generated during this process, that is, CH_4, C_2H_6, C_3H_8.[20] Thus, a highly effective and low-cost hydrogen/hydrocarbon separation is requested for pure hydrogen gas.

In the past decade, the CHA-type zeolite membranes have been theoretically and experimentally studied for gas separations.[21,22] SSZ-13, an aluminosilicate zeolite with CHA-type topology, has a three-dimensional pore system with eight-membered-ring windows with size of 3.8×3.8 $Å^2$.[20] An appropriate window size is necessary for allowing the permeation of H_2 (2.9 Å) while reducing the entrance probability of CH_4 (3.8 Å), C_2H_6 (4.1 Å), and C_3H_8 (4.3 Å) into zeolite pores. Most SSZ-13 zeolites were prepared in micron scale thickness (1–3 μm) membranes according to conventional hydrothermal synthesis methods. The gas permeance was limited on thick zeolite membranes, which is

Huazhen Rong and Yixing Guan contributed equally to this work.

This is an open access article under the terms of the Creative Commons Attribution License, which permits use, distribution and reproduction in any medium, provided the original work is properly cited.
© 2022 The Authors. *Aggregate* published by SCUT, AIEI, and John Wiley & Sons Australia, Ltd.

26924560, 2022, 6, Downloaded from https://onlinelibrary.wiley.com/doi/10.1002/agt2.275 by Test, Wiley Online Library on [25/01/2023]. See the Terms and Conditions (https://onlinelibrary.wiley.com/terms-and-conditions) on Wiley Online Library for rules of use; OA articles are governed by the applicable Creative Commons License

not favorable for industrial production that both high selectivity and high permeance are in demand. An increase in gas permeance is enabled by the reduction of membrane thickness.[23]

Three methods to reduce the thicknesses of zeolite membranes have been reported: (1) additive-regulated crystallization,[24] (2) seeded growth using two-dimensional zeolites,[25,26] and (3) gel-less synthesis.[27,28] The gel-based method is facile and more cost-effective than the former two: nontoxic or uncomplex reagents are needed for zeolite formation. The variation of gel properties can easily control the membrane crystallization. Less gel can avoid the eutrophication effect during the transformation of Si and Al sources into zeolite crystals. In this way, thin zeolite membranes can be produced in the gel-less precursors. One recent example was reported by Zhang and coworkers who synthesized 0.7–1.7 μm SSZ-13 zeolite membranes by manipulating the seed concentration in the dip-coating suspension.[28] In spite of the above success, the following issue still needs to be resolved: defects in gel-less derived membranes should be minimized or even avoided while reducing the thickness by the gel-less method.

In this work, we developed an alternative approach of dual templates assisted gel conversion for synthesizing ultra-thin SSZ-13 zeolite membranes. *N*,*N*,*N*-trimethyl-1-adamantammonium hydroxide (TMAdaOH) and tetraethylammonium hydroxide (TEAOH) were used as organic templates which were verified to direct the formation of the SSZ-13 zeolite membrane.[9,29] The specific effects of TMAdaOH and TEAOH in the membrane crystallization were investigated by composition-varied synthesis gels. The impregnation method was used to transfer the synthesis gel to the seeded porous alumina disc. The gel layer was optimized and crystallized into a submicron membrane under a steam atmosphere. The prepared membranes of SSZ-13 zeolite were subsequently applied for gas permeation of H_2/C_2H_6 and H_2/C_3H_8 for evaluation of hydrogen separation ability.

2 | EXPERIMENTAL SECTION

2.1 | Chemicals

Sodium hydroxide (NaOH, >97%) and sodium aluminate ($NaAlO_2$, Chemically Pure) were received from Beijing Chemical Reagent Company and Sinopharm Chemical Reagent Co. Ltd, China. Aluminum hydroxide ($Al(OH)_3$, ≥99%, Alfa), Ludox AS-40 colloidal silica (SiO_2, 40 wt% suspension in water, Sigma-Aldrich), TMAdaOH (25 wt%, Innochem) and TEAOH (25 wt%, Sigma-Aldrich) aqueous solutions were purchased. The solvent was deionized water. Porous Al_2O_3 discs (diameter of 28 mm, thickness of 3 mm, porosity of 40%, and pore size of 1–3 μm) were used as the supports and they were supplied by Guangdong Yuli Electronic Co. Ltd (China). The discs were smoothed by 500, 1000, and 1500-mesh sand papers, cleaned with deionized water, and then dried at 100°C overnight for subsequent uses.

2.2 | Preparation of SSZ-13 seeds for substrate seeding

The SSZ-13 seeds were prepared in a synthesis solution and the molar ratio was 1.0TMAdaOH:0.62NaOH:0.41$NaAlO_2$:9.67SiO_2:218.2H_2O according to our recent publication.[21] Briefly, NaOH and $NaAlO_2$ were mixed with water to form a clear solution, and then TMAdaOH solution was added. After stirring at room temperature for 1 h, Ludox AS-40 colloidal silica was dropped into the above solution, and the stirring lasted for 6 h. This solution sealed in a 50 mL Teflon-lined autoclave was subjected to crystallization at 160°C for 6 d. The yielded suspension was repetitively centrifuged and washed (18,000 rpm and 20 min for each run) until the supernatant was almost neutral. The cleaned suspension was dried by freeze-drying and weighed to get its mass. The seeds were dispersed in deionized water to give 1.0 wt% solution. Half-height Al_2O_3 disc was immersed into 1.0 wt% seed solution with polished surface downward for 30 s to seed the disc. The wet disc was thermally dried at 85°C for 30 min and this procedure was repeated if another seeding run was required. The surface of the seeded layer was smoothed using a gloved finger.

2.3 | Synthesis of SSZ-13 zeolite membranes

SSZ-13 zeolite membranes were synthesized by steam-assisted conversion of surface gels. The synthesis gels for the membranes were prepared with chemical compositions of *x*TMAdaOH:*y*TEAOH:1.8NaOH:0.2$Al(OH)_3$:7.4SiO_2:795H_2O (*x* ranged from 0 to 2.0, *y* was ranged from 0 to 2.0). The preparation procedure for the synthesis gel using the sources of template, silica, and alumina, was the same as that for the seeds. The seeded discs were immersed in the synthesis gel for 30 s to coat gel layers on the surfaces of seeded discs. Then, the gel-coated disc was placed in a Teflon holder with gel layer facing down. The held disc was transferred into a 50 mL autoclave and 0.2 mL water was added at its bottom. The autoclave was placed in a preheated static oven at 160°C for different time durations. The prepared membranes were calcined at 550°C for 6 h (heating ramp: 1.0°C min^{-1}) in air to remove the organic templates.

2.4 | Characterizations

The crystalline structures of SSZ-13 zeolite seeds and membranes were identified by X-ray diffractions (XRD) on a Rigaku SmartLab X-ray diffractometer. The working conditions were λ = 1.5418 Å for Cu-Kα radiation, 40 kV for the voltage, and 30 mA for the current. SEM images of zeolite seeds and membranes were obtained on field-emission scanning electron microscope (FE-SEM, SU-8010, Hitachi) which was equipped with energy-dispersive X-ray spectroscopy (EDX) for measuring Si/Al ratios of the membranes.

26924560, 2022, 6, Downloaded from https://onlinelibrary.wiley.com/doi/10.1002/agt2.275 by Test, Wiley Online Library on [25/01/2023]. See the Terms and Conditions (https://onlinelibrary.wiley.com/terms-and-conditions) on Wiley Online Library for rules of use; OA articles are governed by the applicable Creative Commons License

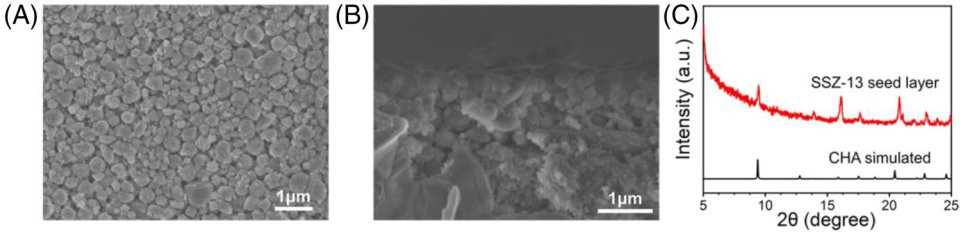

FIGURE 1 SEM images from top (A) and (B) side views for SSZ-13 seed layer, and (C) XRD pattern of SSZ-13 seed layer on porous alumina disc

2.5 | Gas separations

The gas permeation tests of H_2, C_2H_6, and C_3H_8 were carried out on the SSZ-13 zeolite membranes. The SSZ-13 membrane was first placed in a module and then tightly sealed using Teflon O-rings. The effective area of the membrane was 2.54 cm^2. The membrane module was subsequently connected with the system of gas flow. H_2, C_2H_6, and C_3H_8 single gases of 60 mL min^{-1}, and H_2/C_2H_6 and H_2/C_3H_8 binary gases of 60 mL min^{-1}(each gas flow was 30 mL min^{-1}) were introduced at the entry side of the membrane. Argon gas of 50 mL min^{-1} in flow rate swept the back side of the membrane to carry the permeated gas for analysis. Feed and permeate gas concentrations were online analyzed using gas chromatography (Agilent Technologies, 7890B, TCD detector). Before data analysis, the gas permeation was required to reach the steady state. To get a reproducible result, the test was repeated five times under each condition for each membrane. The subsequent calculation was based on this average value. Gas permeances of P and separation factor of S were derived according to the two equations below:

$$P_i = \frac{F_i}{A \times \Delta p} \quad (1)$$

$$S = \frac{y_i/y_j}{x_i/x_j} \quad (2)$$

where P_i (mol m^{-2} s^{-1} Pa^{-1}) is permeance of gas i (H_2, C_2H_6 or C_3H_8), F_i (mol s^{-1}) is flux of gas i, A (m^2) is effective membrane area, and Δp (Pa) is pressure drop of gas i. x_i and x_j are molar fractions of i and j in the feed, y_i and y_j are molar fractions of i and j in the permeate.

3 | RESULTS AND DISCUSSION

3.1 | Monotemplating synthesis of SSZ-13 membranes

SSZ-13 zeolite membranes were attempted to be synthesized by monotemplates of TMAdaOH or TEAOH on the seeded porous alumina discs (Figure 1), and they were characterized by XRD and scanning electron microscopy (SEM). Figures 2 and 3 show the XRD patterns and SEM images of the synthesized membranes with the synthesis gels in molar ratios of xTMAdaOH:0.0TEAOH:1.8NaOH:0.2Al(OH)$_3$:7.4SiO_2:795H_2O (x = 0.5, 1.0, 1.5, 2.0) (the membranes are labeled as M-0.5-0, M-1.0-0, M-1.5-0, M-2.0-0). As we can see in Figure 2, all membranes contain diffractions at 9.4° which belongs to the (100) lattice plane of

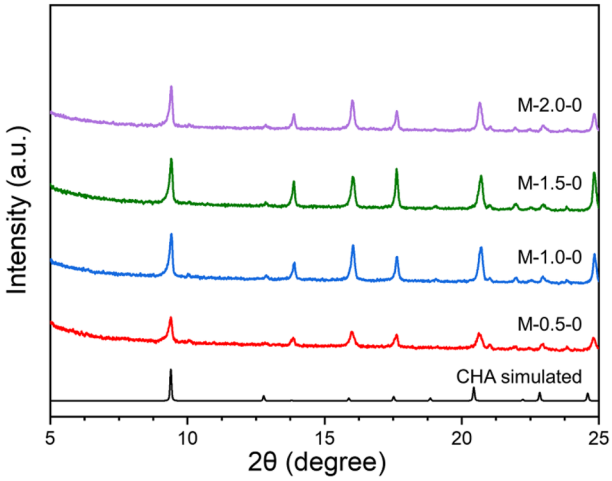

FIGURE 2 XRD patterns of SSZ-13 membranes synthesized in the gels with varied TMAdaOH concentrations at 160°C for 24 h

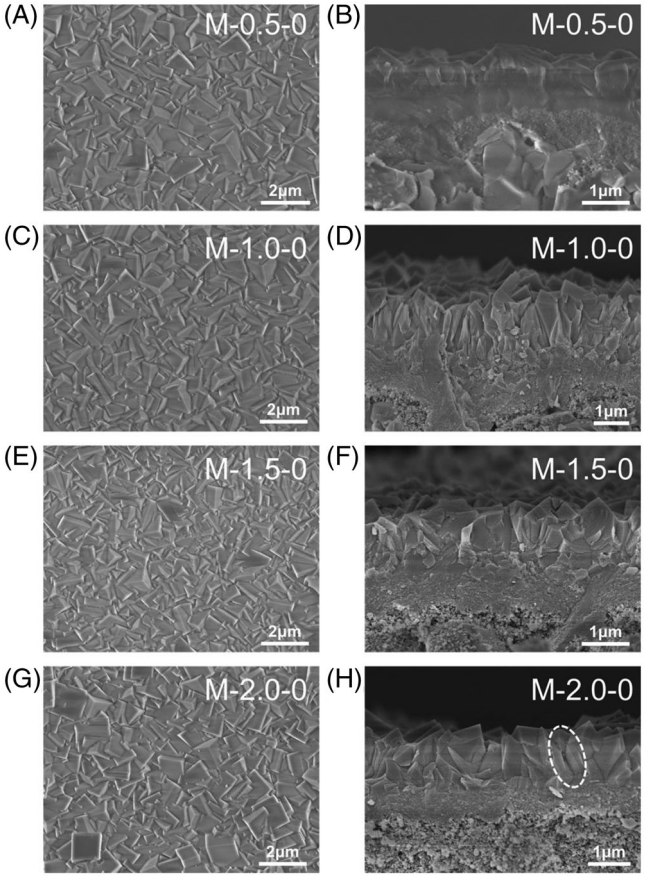

FIGURE 3 SEM images from top (A, C, E, G) and side (B, D, F, H) views for the membranes of SSZ-13 synthesized in the gels with varied TMAdaOH concentrations of x = 0.5 (A, B), 1.0 (C, D), 1.5 (E, F), 2.0 (G, H) at 160°C for 24 h (the gap is marked in a circle in (H))

26924560, 2022, 6, Downloaded from https://onlinelibrary.wiley.com/doi/10.1002/agt2.275 by Test, Wiley Online Library on [25/01/2023]. See the Terms and Conditions (https://onlinelibrary.wiley.com/terms-and-conditions) on Wiley Online Library for rules of use; OA articles are governed by the applicable Creative Commons License

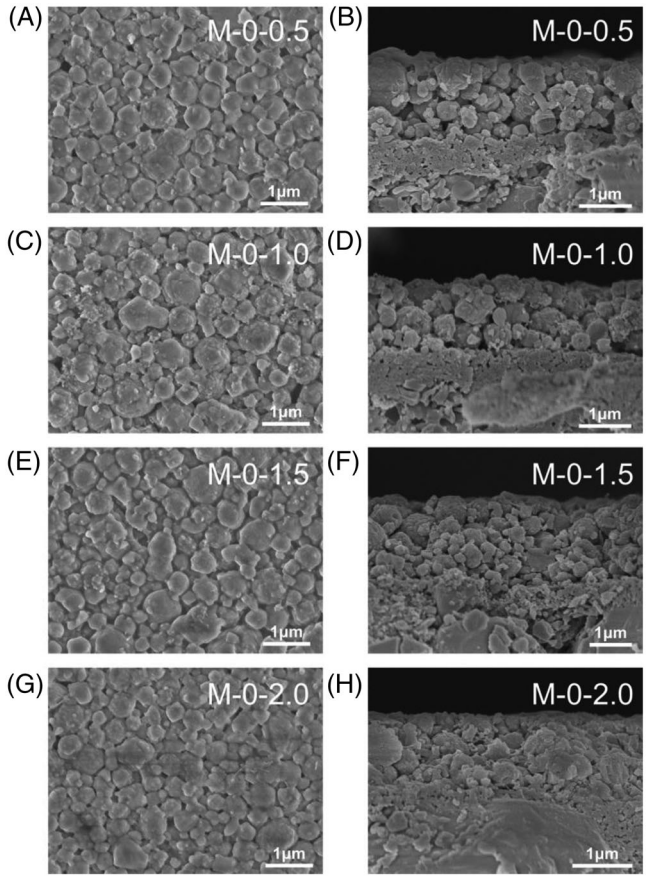

FIGURE 4 SEM images from top (A, C, E, G) and side (B, D, F, H) views for SSZ-13 membranes synthesized in the gels with varied TEAOH concentrations of $y = 0.5$ (A, B), 1.0 (C, D), 1.5 (E, F), 2.0 (G, H) at 160°C for 24 h

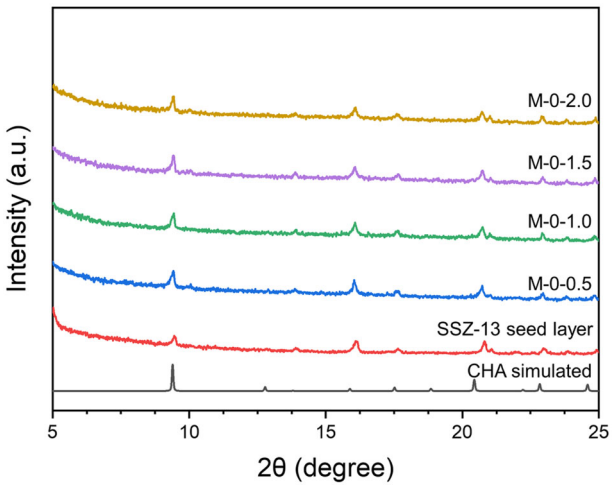

FIGURE 5 XRD patterns of SSZ-13 membranes synthesized in the gels with varied TEAOH concentrations at 160°C for 24 h

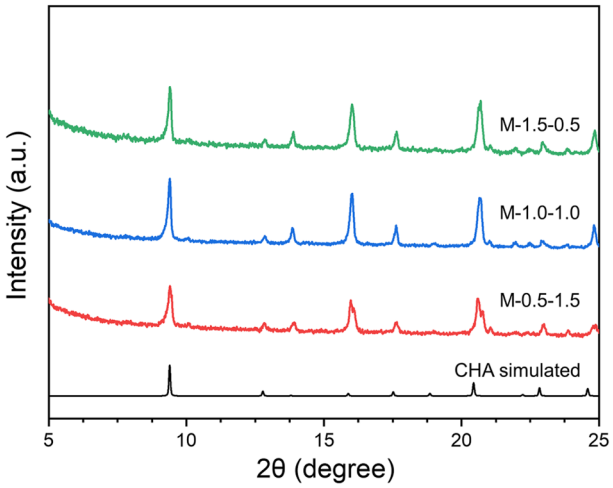

FIGURE 6 XRD patterns of SSZ-13 membranes synthesized in dual-template gels with varied TMAdaOH:TEAOH ratios at 160°C for 24 h

the CHA-type zeolite. This hints that TMAdaOH as the template is able to direct the zeolite to form SSZ-13. However, low TMAdaOH concentration usually reduces the membrane crystallinity (M-0.5-0, Figure 2), comparable to the seeds (Figure 1C). As shown in the top-view SEM images (Figure 3A,C,E,G), regular- and uniform-sized crystals are observed, and the crystals are intergrown into crack-free membranes. The side-view SEM images (Figure 3B,D,F,H) show that the crystals are grown in a side-by-side fashion and the thicknesses of the membranes are uniform. However, with an increase in TMAdaOH concentration, the degree of crystal intergrowth is reduced and some crystal-crystal gaps are observed (Figure 3H). SEM results indicate that TMAdaOH can promote the zeolite growth to form an SSZ-13 membrane, but excess TMAdaOH often results in the gap emergence via crystal mismatch during the crystallization.

Figures 4 and 5 show the SEM images and XRD patterns of the synthesized membranes with the monotemplate of TEAOH in the synthesis gels of 0.0T-MAdaOH:*y*TEAOH:1.8NaOH:0.2Al(OH)$_3$:7.4SiO$_2$:795H$_2$O ($y = 0.5$, 1.0, 1.5, 2.0) (the membranes are labeled as M-0-0.5, M-0-1.0, M-0-1.5, M-0-2.0). As we can see in Figure 4, most particles on the support are isolated from each other no matter how much TEAOH is used. Compared with the seeds (Figure 1), we can see that with an increase in TEAOH concentration, some dissolution is observed on the surface of seed particles after steam treatment, probably due to the increased alkalinity. Although some diffraction peaks are detected (Figure 5), the XRD patterns look similar to that of the seeds. From the above results, we can infer that TEAOH is an inappropriate template for the crystallization of the SSZ-13 membrane and it can slow down the growth of SSZ-13 crystals in comparison to TMAdaOH.

3.2 | Dual-templating synthesis of SSZ-13 membranes

The SSZ-13 zeolite membranes were synthesized in the presence of both TMAdaOH and TEAOH templates. Figures 6 and 7 show the XRD patterns and SEM images of the synthesized membranes in the gels with molar ratios of *x*T-MAdaOH:*y*TEAOH:1.8NaOH:0.2Al(OH)$_3$:7.4SiO$_2$:795H$_2$O (x:y = 0.5:1.5, 1.0:1.0, 1.5:0.5) (the membranes are labeled as M-0.5-1.5, M-1.0-1.0, M-1.5-0.5). The XRD patterns in Figure 6 show that pure-phase SSZ-13 zeolites are crystallized in the gels with TMAdaOH and TEAOH in different ratios. This observation is in agreement with the aforementioned result that TMAdaOH can structurally direct the formation of SSZ-13. The top-view SEM image of M-0.5-1.5 in Figure 7A shows that SSZ-13 nanoparticles with cube-like

26924560, 2022, 6, Downloaded from https://onlinelibrary.wiley.com/doi/10.1002/agt2.275 by Test, Wiley Online Library on [25/01/2023]. See the Terms and Conditions (https://onlinelibrary.wiley.com/terms-and-conditions) on Wiley Online Library for rules of use; OA articles are governed by the applicable Creative Commons License

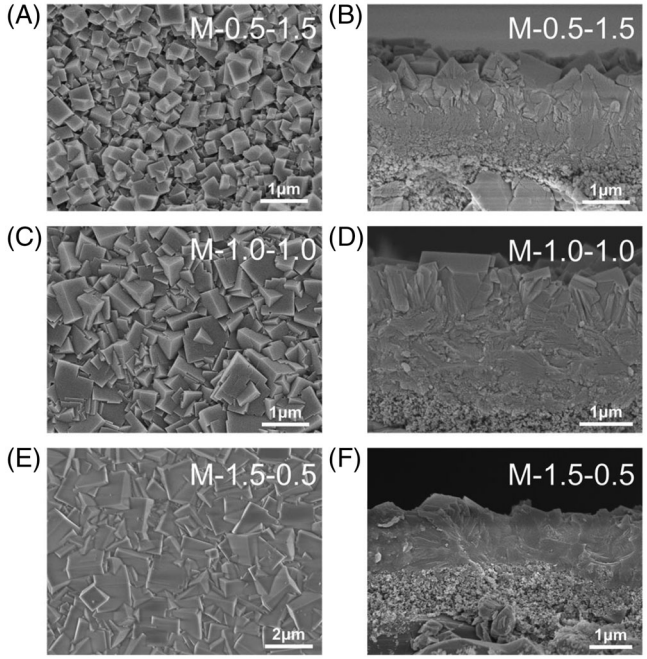

FIGURE 7 SEM images from top (A, C, E) and side (B, D, F) views for SSZ-13 membranes synthesized in dual-template gels with varied TMAdaOH:TEAOH ratios of x:y = 0.5:1.5 (A, B), 1.0:1.0 (C, D), 1.5:0.5 (E, F) at 160°C for 24 h

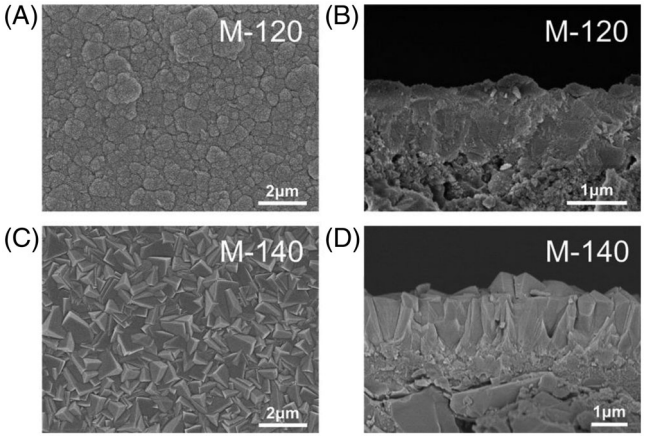

FIGURE 8 SEM images from top (A, C) and side (B, D) views for the membranes of SSZ-13 zeolite synthesized in the gels with dual templates of TMAdaOH:TEAOH = 1.5:0.5 at varied crystallization temperatures (120°C (A, B), 140°C (C, D); the resultant membranes are labeled as M-120, M-140) for 24 h

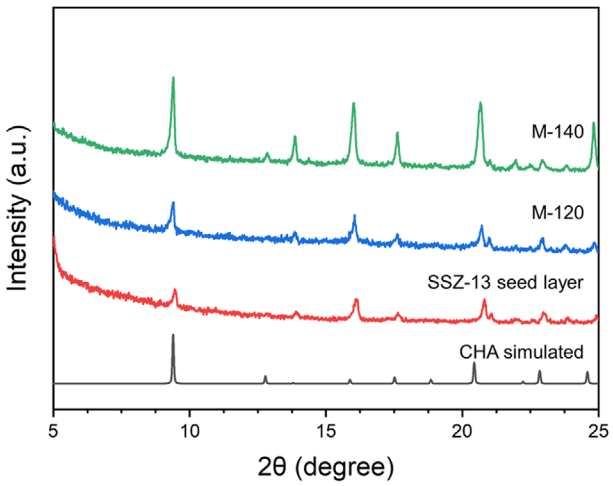

FIGURE 9 XRD patterns for the membranes of SSZ-13 zeolite synthesized in the gels with dual templates of TMAdaOH:TEAOH = 1.5:0.5 at varied crystallization temperatures (120°C, 140°C; the resultant membranes are labeled as M-120, M-140) for 24 h

morphology and in size of 300–500 nm are loosely deposited on the support. More addition of TEAOH than TMAdaOH reduces the growth rate, leading to the yield of small crystals. The reduced rate concurrently results in the loose stacking of particles, which can be seen from the side view in Figure 7B. When the ratio of templates is 1.0:1.0, the crystal size of SSZ-13 is about 1000 nm and the crystals obviously tend to grow together. The increase of TMAdaOH accelerates crystal growth and consequently leads to crystal intergrowth (Figure 7C). However, small gaps still exist between crystals (Figure 7D), indicating that much TEAOH still plays the role of growth inhibitor. As shown in Figure 7E, the crystals in size of 1500 nm are well intergrown when the ratio of TMAdaOH:TEAOH equals to 1.5:0.5. The surface becomes flat and no cracks are visible, giving a continuous membrane. The side view (Figure 7F) also shows that grain boundaries in the zeolite layer are healed and the layer thickness is considerably uniform. Based on the above results, the individual roles of TMAdaOH and TEAOH are tentatively concluded in the following: TMAdaOH serves as the structure directing agent for zeolite formation, and TEAOH acts as the growth modulating agent to regulate SSZ-13 crystallization. With optimal dual templates, high-quality SSZ-13 zeolite membranes can be synthesized in Si/Al ratio of 33(±4) which is little dependent on the substrate (Si/Al of 37 for the gel).

3.3 | Temperature effect on SSZ-13 membrane crystallization

As shown in Figure 8, the SSZ-13 membranes were synthesized at 120°C and 140°C with dual templates of TMAdaOH:TEAOH = 1.5:0.5 for 24 h. At 120°C, the seeds experience slow crystallization in the surface gel. Thus, the particles exhibit spherical shapes like the seeds, but with slightly larger sizes (300–500 nm) (Figure 8A). The XRD pattern in Figure 9 shows that the crystallinity of the membrane (M-120) is not significantly improved in comparison to the seed layer, indicating that the gel is not fully converted into the zeolite. When the crystallization temperature is increased to 140°C, the crystallinity of the resultant membrane (M-140) is significantly improved (Figure 9). The particles after crystallization become regular and cubic, and they are enlarged to 1000–1500 nm (Figure 8C). Increasing the temperature also facilitates the crystal intergrowth, shown by the polycrystalline membrane in Figure 8D. The few gaps in the membrane can be avoided if the seeds are subjected to crystallization at 160°C (Figure 7E,F). At high temperatures, the adjacent crystals are grown together to give a continuous layer, and this layer is firmly anchored onto the support.

26924560, 2022, 6, Downloaded from https://onlinelibrary.wiley.com/doi/10.1002/agt2.275 by Test, Wiley Online Library on [25/01/2023]. See the Terms and Conditions (https://onlinelibrary.wiley.com/terms-and-conditions) on Wiley Online Library for rules of use; OA articles are governed by the applicable Creative Commons License

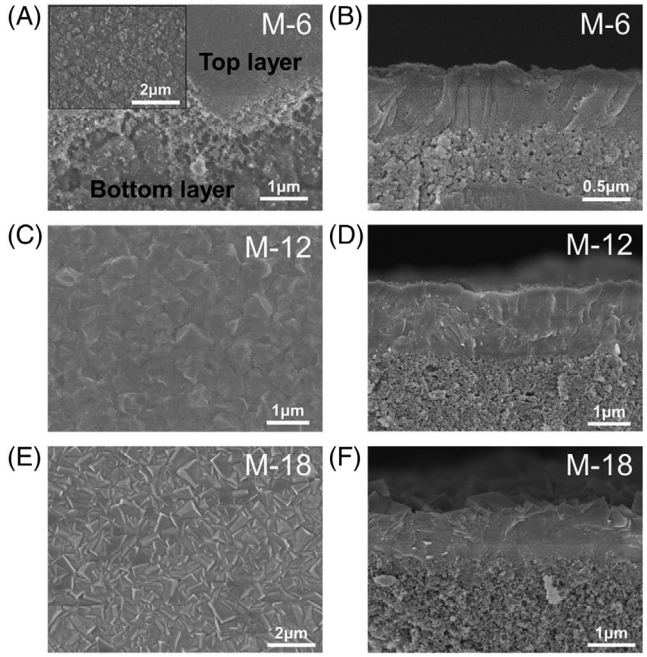

FIGURE 10 SEM images from top (A, C, E) and side (B, D, F) views for the membranes of SSZ-13 zeolite synthesized in the dual-template gel (TMAdaOH:TEAOH = 1.5:0.5) at 160°C for different crystallization times (6 h (A, B), 12 h (C, D), 18 h (E, F), and the corresponding membranes are labeled as M-6, M-12, M-18). The inset in (A) shows an enlarged view of the bottom layer

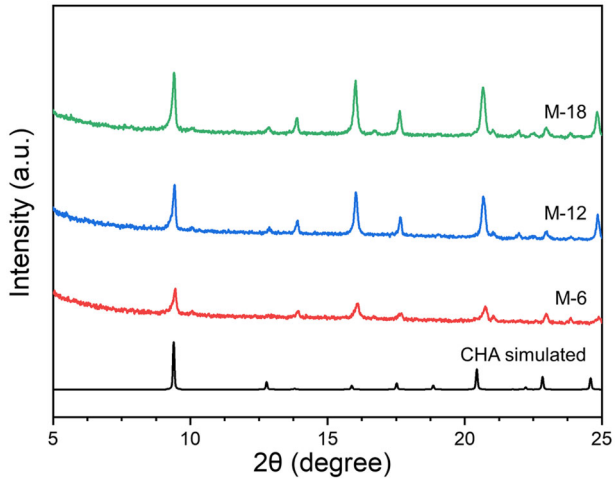

FIGURE 11 XRD patterns for the membranes of SSZ-13 zeolite synthesized in the dual-template gel (TMAdaOH:TEAOH = 1.5:0.5) at 160°C for different crystallization times (6, 12, 18 h, and the corresponding membranes are labeled as M-6, M-12, M-18)

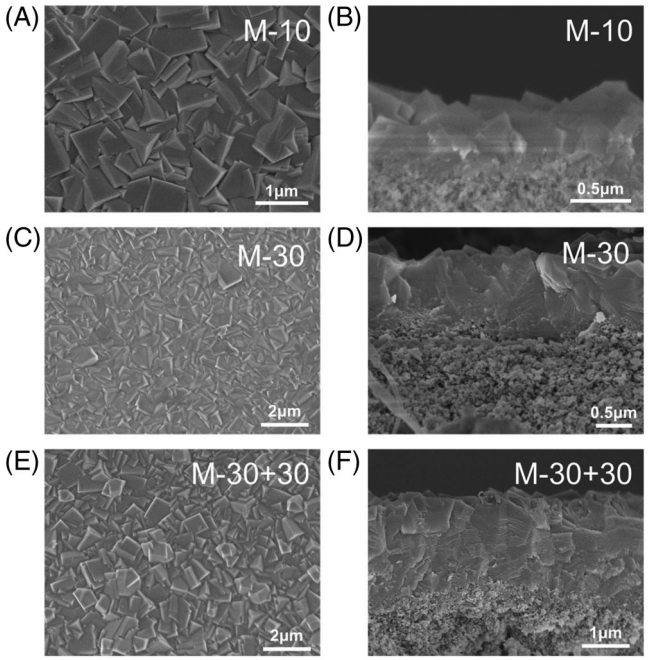

FIGURE 12 SEM images from top (A, C, E) and side (B, D, F) views for SSZ-13 membranes synthesized in amount-varied gels via changing the impregnation time of 10 s (A, B), 30 s (C, D), 30 s + 30 s (E, F) (synthesis gel of 1.5TMAdaOH:0.5TEAOH:1.8NaOH:0.2Al(OH)$_3$:7.4SiO$_2$:795H$_2$O, temperature of 160°C, crystallization time of 24 h)

3.4 | Crystallization process of SSZ-13 membrane

Time-dependent crystallization was followed to elucidate the growth process of the membrane of SSZ-13 zeolite (the gel composition is 1.5TMAdaOH:0.5TEAOH:1.8NaOH:0.2Al(OH)$_3$:7.4SiO$_2$:795H$_2$O, T = 160°C). The SEM image in Figure 10A shows that an amorphous layer covers the top surface of the disc and this layer is partially cleaved from the support after sonication, indicating that it is impossible to convert all the gel into crystals within 6 h crystallization (M-6). Underneath the top layer (inset in Figure 10A,B), seeds grow up with a tendency to fill the gaps between them. After crystallization for 12 h (M-12), most of the amorphous layer disappears and cubic-shape crystals evolve (Figure 10C). From the side view of the SEM image in Figure 10D, an interface between the layer and the support is clearly seen, suggesting that the gel layer is crystallized into zeolite. As crystallization progresses, the gel is consecutively consumed by the seeds; as a consequence, the crystals become larger and intergrow together. When the crystallization time is extended to 18 h (M-18), almost all the gel is converted to the zeolite, as shown by the regular crystals in Figure 10E. The crystal size is around 1000 nm. The progressive crystallization results in a continuous zeolite layer (Figure 10F). The layer thickness (~1200 nm) is comparable to the membrane at 24 h. Crystallization for 24 h is intended to heal the small defects that cannot be observed by SEM. The XRD patterns in Figure 11 show that the crystallinity of SSZ-13 zeolite membranes increases with the synthesis time, which is consistent with the SEM observation.

3.5 | Synthesis of thin SSZ-13 membrane

The gel thickness is first adjusted by impregnating the seeded support with the synthesis gel at different times. And then, the gel-containing seeds are thermally treated in a steam atmosphere. The top views of SEM images (Figure 12A,C,E) show that SSZ-13 crystals completely cover the support, forming continuous and crack-free membranes. The side views of SEM images (Figure 12B,D,F) show that the membrane thickness is linearly increased with the time of gel impregnation: the thickness is around 450 nm after 10 s of impregnation (the membrane is labeled as M-10) and it increases to 1200 nm if the impregnation time is 30 s

26924560, 2022, 6, Downloaded from https://onlinelibrary.wiley.com/doi/10.1002/agt2.275 by Test, Wiley Online Library on [25/01/2023]. See the Terms and Conditions (https://onlinelibrary.wiley.com/terms-and-conditions) on Wiley Online Library for rules of use; OA articles are governed by the applicable Creative Commons License

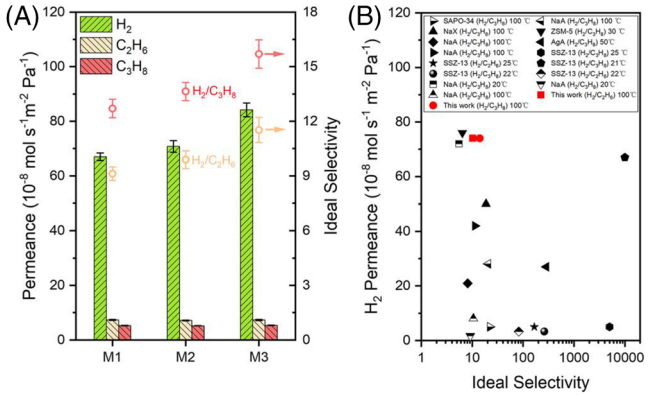

FIGURE 13 (A) H_2, C_2H_6, and C_3H_8 permeances and ideal selectivity for single gases on thin membranes of SSZ-13 zeolite (M1, M2, M3 were synthesized by the same method, thicknesses of ~500 nm) tested at 120 kPa (feed pressure) and 100°C and (B) separation performance summary of H_2 permeance and ideal selectivity (H_2/C_2H_6, H_2/C_3H_8) for zeolite membranes from the literature

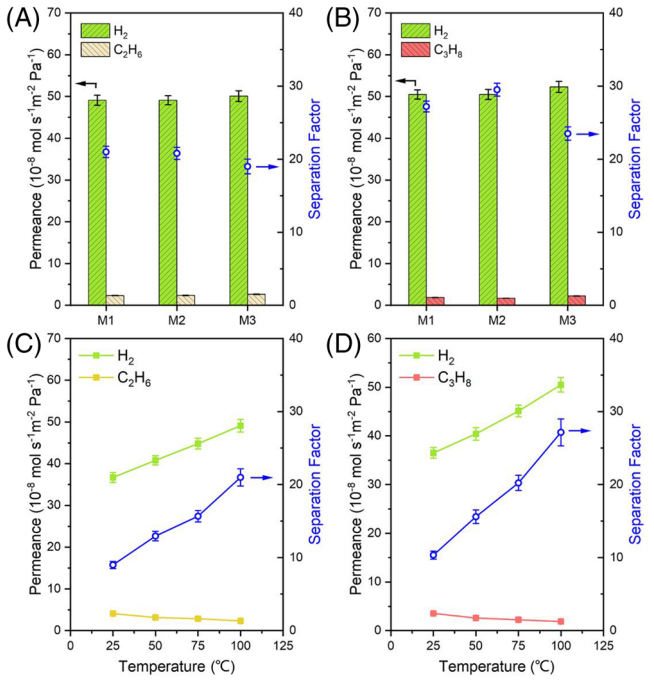

FIGURE 14 H_2, C_2H_6, and C_3H_8 permeances and separation factors for mixture gases (50%:50% in volume) of (A) H_2/C_2H_6 and (B) H_2/C_3H_8 on thin membranes of SSZ-13 zeolite (M1, M2, and M3 were synthesized by the same method, thicknesses of ~500 nm) tested at 120 kPa (feed pressure) and 100°C. Gas permeances and separation factors for mixture (C) H_2/C_2H_6 and (D) H_2/C_3H_8 gases at different temperatures tested at 120 kPa (feed pressure)

(M-30). A thick membrane of 1800 nm is yielded when 30 s of impregnation is repeated (M-30+30). In this method, the nutrients of silica and alumina from the surface gel are fully converted into the zeolite membrane. This accounts for the fact that the thickness of the membrane is determined by the gel layer. The above result shows that this method can facilely control the membrane thickness and it is advantageous over the conventional hydrothermal route. Zeolite membranes with reduced thicknesses are obtained and thin membranes are beneficial for fast gas permeation in the membrane separation process.

3.6 | Gas separation

Gas separation properties of H_2 from C_2H_6 and C_3H_8 were investigated on the thin SSZ-13 zeolite membranes according to the standard method of Wicke–Kallenbach. Three membranes (M1, M2, M3) were synthesized with thicknesses around 500 nm using the impregnated gels containing dual templates (TMAdaOH:TEAOH = 1.5:0.5, impregnation time: 10 s, crystallization temperature: 160°C, crystallization time: 24 h). The quality of the as-synthesized membrane (before activation) was priorly checked by single gas permeation of H_2, C_2H_6, and C_3H_8. The measured H_2 permeance of 0.4×10^{-8} mol s^{-1} m^{-2} Pa^{-1}(100°C, 120 kPa) is substantially lower than bare Al_2O_3 disc (804×10^{-8} mol s^{-1} m^{-2} Pa^{-1}), conveying that the zeolite membrane is well deposited on the support. The detected permeances of 0.14×10^{-8} mol s^{-1} m^{-2} Pa^{-1} and 0.11×10^{-8} mol s^{-1} m^{-2} Pa^{-1} for C_2H_6 and C_3H_8 imply the defect existence; nevertheless, the permeation through defects will contribute a small fraction of membrane permeation after activation (ideal selectivity: 2.9 and 3.7 for as-synthesized membrane, 1.09 and 1.54 for bare support, of H_2/C_2H_6 and H_2/C_3H_8, respectively). The data of gas permeation (permeance, selectivity) measured at 100°C and 120 kPa for the activated membranes (calcined in air to remove templates) are displayed in Figure 13A. The three membranes of M1, M2, and M3 have similar permeance and selectivity: the average permeances for single H_2, C_2H_6, and C_3H_8 gases are 74.0×10^{-8}, 7.28×10^{-8}, and 5.29×10^{-8} mol s^{-1} m^{-2} Pa^{-1}, respectively. The H_2/C_2H_6 and H_2/C_3H_8 ideal selectivities derived from single gases are 10.2 and 14.0, respectively. Referencing the as-synthesized membranes, the activated membranes exhibit two-magnitude higher H_2 permeance and greater gas selectivity beyond Knudsen diffusion selectivity (3.9 and 4.7 for H_2/C_2H_6 and H_2/C_3H_8), showing that gas transports mainly take place in SSZ-13 zeolite pores. The ideal selectivity of >10 for H_2/C_2H_6 and H_2/C_3H_8 on the SSZ-13 membrane can be explained with the diffusion principle: H_2 (2.9 Å) molecule is smaller than C_2H_6 (4.1 Å) and C_3H_8 (4.3 Å), and higher diffusivity is expected for H_2.[30] This means that H_2 molecules are easier to enter the SSZ-13 zeolite pores (the crystallographic pore size of 3.8 Å), thereby allowing their preferential diffusion.[31] The diffusion outcome gives selective gas permeation of H_2 over C_2H_6 and C_3H_8 through the membrane. H_2 permeance is larger than those for most zeolite membranes (Figure 13B),[16,32–43] showing that the thin membrane indeed favors fast gas permeation. The moderate selectivity suggests that the defect number should be minimized by more advanced approaches for membrane synthesis or activation since thin membranes have lower tolerance to defects than thick ones. The similarity of gas permeance obtained on M1, M2, and M3 shows that thin SSZ-13 membranes can be reproducibly synthesized.

Further, the thin membranes of SSZ-13 zeolite were studied for the separation of H_2/C_2H_6 and H_2/C_3H_8 mixtures (50%:50% in volume). As shown in Figure 14A,B, the H_2 permeances are 49.4×10^{-8} and 51.1×10^{-8} mol s^{-1} m^{-2} Pa^{-1} for H_2/C_2H_6 and H_2/C_3H_8 mixtures, which are smaller than the values in single-gas permeations. The separation factors are averaged at 20.2 and 26.7 for H_2/C_2H_6 and H_2/C_3H_8, respectively. The phenomenon of separation

26924560, 2022, 6, Downloaded from https://onlinelibrary.wiley.com/doi/10.1002/agt2.275 by Test, Wiley Online Library on [25/01/2023]. See the Terms and Conditions (https://onlinelibrary.wiley.com/terms-and-conditions) on Wiley Online Library for rules of use; OA articles are governed by the applicable Creative Commons License

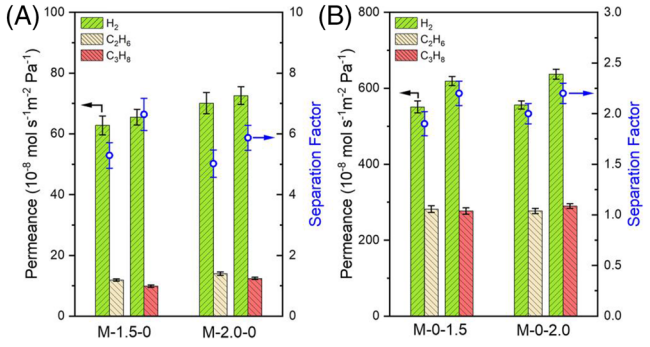

FIGURE 15 H_2, C_2H_6, and C_3H_8 permeances and separation factors for mixture gases (50%:50% in volume) of H_2/C_2H_6 and H_2/C_3H_8 on monotemplate synthesized membranes of SSZ-13 zeolite tested at 120 kPa in feed pressure and 100°C in temperature: (A) TMAdaOH, (B) TEAOH

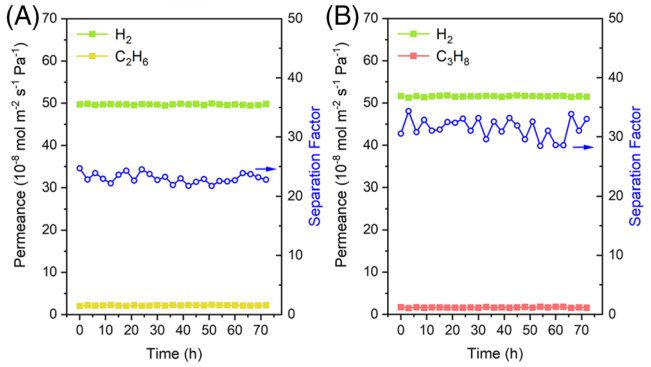

FIGURE 16 H_2, C_2H_6, and C_3H_8 permeances, and separation factors as a function of operation time for mixture gases (50%:50% in volume) of (A) H_2/C_2H_6 and (B) H_2/C_3H_8 on the thin SSZ-13 zeolite membrane measured at 120 kPa (feed pressure) and 100°C

factor higher than ideal selectivity also occurs in another case of H_2/C_3H_8 permeation through the SAPO-34 membrane (CHA-type zeolite, 3.5 μm thick) in the previous report (ideal selectivity of ~26 and separation factor of ~48 at 100°C).[32] The exact reason is unclear till now, but the operation condition (temperature, pressure)[44,45] as one cause can affect H_2 and C_2H_6(C_3H_8) transport by varying gas molecular states at membrane surface or in zeolite pores.[46,47] Temperature-dependent permeation data (Figure 14C,D) show that C_2H_6 and C_3H_8 permeances decrease concurrently with increasing H_2/C_2H_6 and H_2/C_3H_8 separation factors, due to less adsorbed C_2H_6 (C_3H_8) and faster diffused H_2 as the temperature increases. This result offers additional evidence to support the aforementioned hypothesis of diffusion-driven selective H_2 separation from C_2H_6 (C_3H_8) at high temperatures. The permeance of C_2H_6 (2.34×10^{-8} mol s^{-1} m^{-2} Pa^{-1}) is slightly greater than C_3H_8 (1.86×10^{-8} mol s^{-1} m^{-2} Pa^{-1}), presumably because of the kinetic effect that bigger C_3H_8 has higher diffusion resistance. Figure 15 shows gas permeance and separation factor of H_2/C_2H_6 and H_2/C_3H_8 mixtures (50%:50% in volume) on the membranes synthesized by monotemplates of TMAdaOH (Figure 15A) and TEAOH (Figure 15B). The membranes have H_2/C_2H_6 and H_2/C_3H_8 separation factors of 5.3 and 6.6 for M-1.5-0, and 5.0 and 5.9 for M-2.0-0, respectively; inferior to the membrane synthesized by dual templates (Figure 14). Under the same conditions, the separation factors on membranes synthesized by the monotemplate of TEAOH are around 2.0 (Figure 15B). The result comparison advocates the conclusion that dual templates can significantly improve the membrane's continuity.

Time-dependent gas separation was used to examine the membrane stability. Gas permeances and separation factors of H_2/C_2H_6 and H_2/C_3H_8 mixtures (50%:50% in volume) are recorded for 72 h in Figure 16. The permeances and separation factors show small fluctuations: H_2 permeances are around 49.7×10^{-8} mol s^{-1} m^{-2} Pa^{-1} and H_2/C_2H_6 separation factors approximate 23.0 in Figure 16A. The average H_2 permeance is 51.6×10^{-8} mol s^{-1} m^{-2} Pa^{-1} and the mean value of H_2/C_3H_8 separation factor is 31.5 in Figure 16B. Considerably constant permeance and separation factor in the whole measurement indicates that the synthesized ultra-thin SSZ-13 zeolite membrane is quite stable for hydrogen separation from the mixtures of H_2/C_2H_6 and H_2/C_3H_8.

4 | CONCLUSION

The synthesis of ultra-thin and continuous membranes of SSZ-13 zeolite was successfully achieved by the transformation of the surface gels in the presence of dual templates. Systematical investigation of mono and dual templates in membrane crystallization showed that TMAdaOH was an appropriate organic template for directing SSZ-13 zeolite formation and TEAOH served as a growth modulator to regulate crystal intergrowth. The interplay of both organic templates led to the production of continuous membranes without visible cracks. The thickness of the gel layer was controlled by the impregnation method. A 500 nm thick SSZ-13 membrane was successfully synthesized with minimal gel. Gas permeation results revealed that the synthesized submicron membranes possessed good hydrogen separation performances. H_2 permeance approached 84.2×10^{-8} mol s^{-1} m^{-2} Pa^{-1}, superior to most zeolite membranes. The separation factor exceeded 23 for H_2 over C_2H_6 and C_3H_8. This method was also advantageous in maximal material utilization and minimal waste disposal. Superior hydrogen separation and environmental-friendly synthesis shed light on the potential of this approach for the preparation of high-performance zeolite membranes.

ACKNOWLEDGMENTS

We would like to acknowledge the financial support from the National Natural Science Foundation of China (NSFC grant nos. 21971035, 22131004, and U21A20330), the "111" Program (B18012), and the Fundamental Research Funds for the Central Universities (JGPY202103).

CONFLICT OF INTEREST

The authors declare no conflict of interest.

DATA AVAILABILITY STATEMENT

The data that support the findings of this study are available from the corresponding author upon reasonable request.

ORCID

Xiaoqin Zou https://orcid.org/0000-0002-8401-5538

REFERENCES

1. X. Lin, H. Kita, K. Okamoto, *Chem. Commun.* **2000**, *19*, 1889.

26924560, 2022, 6, Downloaded from https://onlinelibrary.wiley.com/doi/10.1002/agt2.275 by Test, Wiley Online Library on [25/01/2023]. See the Terms and Conditions (https://onlinelibrary.wiley.com/terms-and-conditions) on Wiley Online Library for rules of use; OA articles are governed by the applicable Creative Commons License

2. J. Gascon, F. Kapteijn, B. Zornoza, V. Sebastián, C. Casado, J. Coronas, *Chem. Mater.* **2012**, *24*, 2829.
3. M. Yu, R. D. Noble, J. L. Falconer, *Acc. Chem. Res.* **2011**, *44*, 1196.
4. G. Bernardo, T. Araújo, T. da Silva Lopes, J. Sousa, A. Mendes, *Int. J. Hydrogen Energy* **2020**, *45*, 7313.
5. M. Tagliabue, D. Farrusseng, S. Valencia, S. Aguado, U. Ravon, C. Rizzo, A. Corma, C. Mirodatos, *Chem. Eng. J.* **2009**, *155*, 553.
6. L.-H. Chen, M.-H. Sun, Z. Wang, W.-M. Yang, Z.-K. Xie, B.-L. Su, *Chem. Rev.* **2020**, *120*, 11194.
7. M. Wang, M. Li, N. Chang, L. Gao, M. Wang, Y. Zhang, *J. Membr. Sci.* **2018**, *565*, 311.
8. K. Kida, Y. Maeta, K. Yogo, *Sep. Purif. Technol.* **2018**, *197*, 116.
9. S. Araki, H. Ishii, S. Imasaka, H. Yamamoto, *Microporous Mesoporous Mater.* **2020**, *292*, 109798.
10. Y. Zheng, N. Hu, H. Wang, N. Bu, F. Zhang, R. Zhou, *J. Membr. Sci.* **2015**, *475*, 303.
11. S. Yang, Z. Cao, A. Arvanitis, X. Sun, Z. Xu, J. Dong, *J. Membr. Sci.* **2016**, *505*, 194.
12. L. Wang, C. Zhang, X. Gao, L. Peng, J. Jiang, X. Gu, *J. Membr. Sci.* **2017**, *539*, 152.
13. N. Xu, D. Meng, X. Tang, X. Kong, L. Kong, Y. Zhang, H. Qiu, M. Wang, Y. Zhang, *Sep. Purif. Technol.* **2020**, *253*, 117505.
14. E. Kim, S. Hong, E. Jang, J. H. Lee, J. C. Kim, N. Choi, C. H. Cho, J. Nam, S. K. Kwak, A. C. K. Yip, J. Choi, *J. Mater. Chem. A* **2017**, *5*, 11246.
15. C. Zhou, N. Wang, Y. Qian, X. Liu, J. Caro, A. Huang, *Angew. Chem. Int. Ed.* **2016**, *55*, 12678.
16. Y. Li, H. Chen, J. Liu, W. Yang, *J. Membr. Sci.* **2006**, *277*, 230.
17. M. Momirlan, T. N. Veziroglu, *Renewable Sustainable Energy Rev.* **2002**, *6*, 141.
18. S. A. Salaudeen, B. Acharya, M. Heidari, S. M. Al-Salem, A. Dutta, *Energy Fuels* **2020**, *34*, 4828.
19. G. Kolb, S. Keller, M. O'Connell, S. Pecov, J. Schuerer, B. Spasova, D. Tiemann, A. Ziogas, *Energy Fuels* **2013**, *27*, 4395.
20. T. Wu, C. Shu, S. Liu, B. Xu, S. Zhong, R. Zhou, *Energy Fuels* **2020**, *34*, 11650.
21. Z. Li, J. Li, H. Rong, J. Zuo, X. Yang, Y. Xing, Y. Liu, G. Zhu, X. Zou, *J. Am. Chem. Soc.* **2022**, *144*, 6687.
22. X. Wang, T. Zhou, P. Zhang, W. Yan, Y. Li, L. Peng, D. Veerman, M. Shi, X. Gu, F. Kapteijn, *Angew. Chem. Int. Ed.* **2021**, *60*, 9032.
23. H. Rong, J. Zhang, Y. Guan, D. Gai, X. Zou, *ACS Appl. Mater. Interfaces* **2022**, *14*, 26171.
24. L. Yu, A. Holmgren, M. Zhou, J. Hedlund, *J. Mater. Chem. A* **2018**, *6*, 6847.
25. B. Wang, T. Wu, M. Yu, S. Li, R. Zhou, W. Xing, *Small* **2020**, *16*, 2002836.
26. M. Y. Jeon, D. Kim, P. Kumar, P. S. Lee, N. Rangnekar, P. Bai, M. Shete, B. Elyassi, H. S. Lee, K. Narasimharao, S. N. Basahel, S. Al-Thabaiti, W. Xu, H. J. Cho, E. O. Fetisov, R. Thyagarajan, R. F. DeJaco, W. Fan, K. A. Mkhoyan, J. I. Siepmann, M. Tsapatsis, *Nature* **2017**, *543*, 690.
27. T. C. T. Pham, T. H. Nguyen, K. B. Yoon, *Angew. Chem. Int. Ed.* **2013**, *52*, 8693.
28. X. Tang, Y. Zhang, D. Meng, X. Kong, L. Kong, H. Qiu, N. Xu, W. Guo, S. Yang, Y. Zhang, *J. Membr. Sci.* **2021**, *620*, 118920.
29. I. Bull, U. Mueller, US20100950137, **2011**.
30. W. Mei, Y. Du, T. Wu, F. Gao, B. Wang, J. Duan, J. Zhou, R. Zhou, *J. Membr. Sci.* **2018**, *565*, 358.
31. J. Guo, Y. Li, Y. Huang, D. Wang, *J. Nanosci. Nanotechnol.* **2014**, *14*, 6858.
32. Z. Wang, J. Xu, S. Pati, T. Chen, Y. Deng, N. Dewangan, L. Meng, J. Y. S. Lin, S. Kawi, *AIChE J.* **2020**, *66*, e16278.
33. C. Yuan, Q. Liu, H. Chen, A. Huang, *RSC Adv.* **2014**, *4*, 41982.
34. Z.-L. Cheng, Z.-S, Chao, W.-P. Fang, H.-Q. Lin, H.-L. Wan, *Acta Chim. Sin.* **2003**, *61*, 1944.
35. H.-R. Chen, R.-R. Chang, L. Li, W.-H. Yuan, *Acta Phys. Sin.* **2011**, *27*, 241.
36. A. Huang, N. Wang, J. Caro, *J. Membr. Sci.* **2012**, *389*, 272.
37. S. Yang, B. Min, Q. Fu, C. W. Jones, S. Nair, *Angew. Chem. Int. Ed.* **2022**, *61*, e202204265.
38. S. Yang, Y. H. Kwon, D.-Y. Koh, B. Min, Y. Liu, S. Nair, *ChemNanoMat* **2019**, *5*, 61.
39. B. Wang, Y. Zheng, J. Zhang, W. Zhang, F. Zhang, W. Xing, R. Zhou, *Microporous Mesoporous Mater.* **2019**, *275*, 191.
40. X. Chen, W. Yang, J. Liu, L. Lin, *J. Membr. Sci.* **2005**, *255*, 201.
41. W. Yuan, H. Chen, R. Chang, L. Li, *Desalination* **2011**, *273*, 343.
42. Z.-L. Cheng, X.-X. Qin, *Appl. Mech. Mater.* **2014**, *477*, 1481.
43. K. Xu, C. Yuan, J. Caro, A. Huang, *J. Membr. Sci.* **2016**, *511*, 1.
44. W. J. W. Bakker, L. J. P. van den Broeke, F. Kapteijn, J. A. Moulijn, *AIChE J.* **1997**, *43*, 2203.
45. J. H. Dong, Y. S. Lin, W. Liu, *AIChE J.* **2000**, *46*, 1957.
46. R. Zhou, Y. Pan, W. Xing, N. Xu, *Adv. Membr.* **2021**, *1*, 100011.
47. J. Xu, K.-G. Haw, Z. Li, S. Pati, Z. G. Wang, S. Kawi, *React. Chem. Eng.* **2021**, *6*, 52.

How to cite this article: H. Rong, Y. Guan, J. Li, Z. Li, D. Ma, J. Zhang, T. X. Liu, X. Zou, *Aggregate* **2022**, *3*, e275. https://doi.org/10.1002/agt2.275

26924560, 2022, 6, Downloaded from https://onlinelibrary.wiley.com/doi/10.1002/agt2.275 by Test, Wiley Online Library on [25/01/2023]. See the Terms and Conditions (https://onlinelibrary.wiley.com/terms-and-conditions) on Wiley Online Library for rules of use; OA articles are governed by the applicable Creative Commons License